International Journal of Thermophysics, Vol. 22, No. 4, 2001

Thermal Diffusivity and Sound Speed of the Refrigerant R143a (1,1,1-Trifluoroethane)[1]

A. P. Fröba,[2] S. Will,[2,3] and A. Leipertz[2,4]

The thermal diffusivity and the sound speed of the refrigerant R143a (1,1,1-trifluoroethane) have been determined in the temperature range 273 to 346 K by dynamic light scattering (DLS), a method based on the time-resolved analysis of scattered light intensities, which are caused by microscopic density fluctuations in the sample. The results for R143a are discussed in detail in comparison to data available in the literature. With the help of reference data for the thermal conductivity and density, the experimental data of the thermal diffusivity also allow the derivation of the isobaric heat capacity for both phases under saturation conditions.

KEY WORDS: 1,1,1-trifluoroethane; dynamic light scattering; R143a; sound speed; thermal diffusivity.

1. INTRODUCTION

After ten years of research most of the essential data for R134a and for R152a are available. In contrast, a literature survey reveals that only a very limited number of data are available for refrigerant R143a, which for refrigeration purposes is mainly used as a component in the blends R404A (R125/R134a/R143a) and R507 (R125/R143a). This situation holds for equilibrium data and is even more pronounced for transport properties. Only two experimental data sets can be found in the literature for the thermal conductivity of both saturated liquid and vapor [1–3], and data

[1] Paper presented at the Fourteenth Symposium on Thermophysical Properties, June 25–30, 2000, Boulder, Colorado, U.S.A.

[2] Lehrstuhl für Technische Thermodynamik (LTT), Friedrich-Alexander-Universität Erlangen-Nürnberg, Am Weichselgarten 8, D-91058 Erlangen, Germany.

[3] Technische Thermodynamik/Wärme- und Stofftransport (TTWSt), Universität Bremen, FB4, Badgasteiner Straße 1, D-28359 Bremen, Germany.

[4] To whom correspondence should be addressed. E-mail: sek@ltt.uni-erlangen.de

0195-928X/01/0700-1021$19.50/0

for the upper temperature region are only obtained from lower temperature values by extrapolation and are completely lacking for the critical region.

In the present paper the methodological principles of dynamic light scattering (DLS) for the determination of thermal diffusivity and sound speed are briefly reviewed. Then experimental results for R143a are discussed in comparison with the few literature data available.

2. METHOD

In the following, the underlying theory of DLS for bulk fluids is briefly introduced. For a more detailed and comprehensive description the reader is referred to the literature [4–7].

When a fluid sample in macroscopic equilibrium is irradiated by coherent laser light, light scattered from the sample can be observed in all directions. The underlying scattering process is governed by microscopic fluctuations of the thermodynamic properties temperature and pressure, and of species concentration in binary mixtures. The relaxations of these statistical fluctuations follow the same laws which are valid for macroscopic systems. Thus, the decay of temperature fluctuations is governed by the thermal diffusivity a. Pressure fluctuations in fluids are moving with sound speed c_S and their decay is governed by the sound attenuation D_S. In binary fluid mixtures, the decay of fluctuations in concentration is governed by the mutual diffusion coefficient D_{12}.

A typical scattering geometry for light scattering from bulk fluids is shown in Fig. 1. With the scattering angle Θ_s, which defines the angle

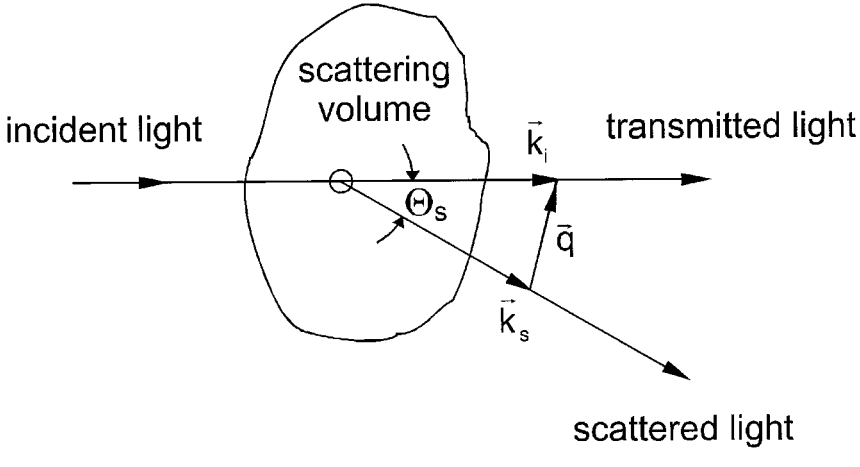

Fig. 1. Scattering geometry: light scattering from bulk fluids.

between the direction of observation and incident light, the scattering vector is determined by $\vec{q} = \vec{k}_i - \vec{k}_s$. Here, the wave vectors of incident and scattered light are represented by $\vec{k}_i$ and $\vec{k}_s$, respectively. Assuming elastic scattering ($k_i \cong k_s$), the modulus of the scattering vector is given by the fluid refractive index n, the laser wavelength in vacuo λ_0, and the scattering angle Θ_s by

$$q = |\vec{k}_i - \vec{k}_s| \cong 2k_i \sin(\Theta_s/2) = \frac{4\pi n}{\lambda_0} \sin(\Theta_s/2) \tag{1}$$

In light scattering experiments the above-mentioned equalization processes result in a temporal modulation of the scattered light intensity. Information about these processes can be derived by a temporal analysis of the scattered light using photon correlation spectroscopy. For heterodyne conditions, where a reference beam is superimposed on the scattered light, the correlation function for the analysis of the temperature fluctuations is described by

$$G^{(2)}(\tau) = A + B \exp(-\tau/\tau_C) \tag{2}$$

From the correlation time τ_C, which is equivalent to the mean life time of the temperature fluctuations observed, the thermal diffusivity a can be calculated by

$$a = \frac{1}{\tau_C q^2} \tag{3}$$

For the measurement of sound speed c_S, the pressure fluctuations are probed. In practice, the frequency ω_S of the sound waves is determined by adding a reference beam, which is shifted relative to the frequency ω_0 of the laser light by $\Delta\omega_M$ applying an acousto-optical modulator. The frequency shift $\Delta\omega_M$ is of the same order of magnitude as the frequency of the sound waves ($\Delta\omega_M \approx \omega_S$). In this case, the correlation function takes the form,

$$G^{(2)}(\tau) = A + B \exp(-\tau/\tau_C) \cos(\Delta\omega\tau) \tag{4}$$

where the sound velocity c_S can be found from the adjusted modulator frequency $\Delta\omega_M$ and the residual detuning $\Delta\omega$ according to

$$c_S = \frac{\omega_S}{q} = \frac{\Delta\omega_M \pm \Delta\omega}{q} \tag{5}$$

Furthermore, the sound attenuation D_S can be determined from the decay time τ_C of the correlation function, Eq. (4), by

$$D_S = \frac{1}{\tau_C q^2} \tag{6}$$

3. EXPERIMENTAL

The experimental setup is shown schematically in Fig. 2. Light from an argon–ion laser operating at a single longitudinal mode at a wavelength of $\lambda_0 = 488$ nm irradiates the refrigerant sample inside a pressure vessel through a quartz window. The laser power was up to 300 mW when working far away from the critical point, and only a few mW in the critical region. The observation direction is given by two apertures at a distance of about 4 m. The scattered light is typically detected at small angles $\Theta_s \sim 3$ to 5°. For large scattering intensities from the sample, the scattered reference light from the cell windows is not sufficient to realize heterodyne conditions. Here, an additional reference beam is added. To this end, part of the incident laser light is split by a glass plate and superimposed on the scattered

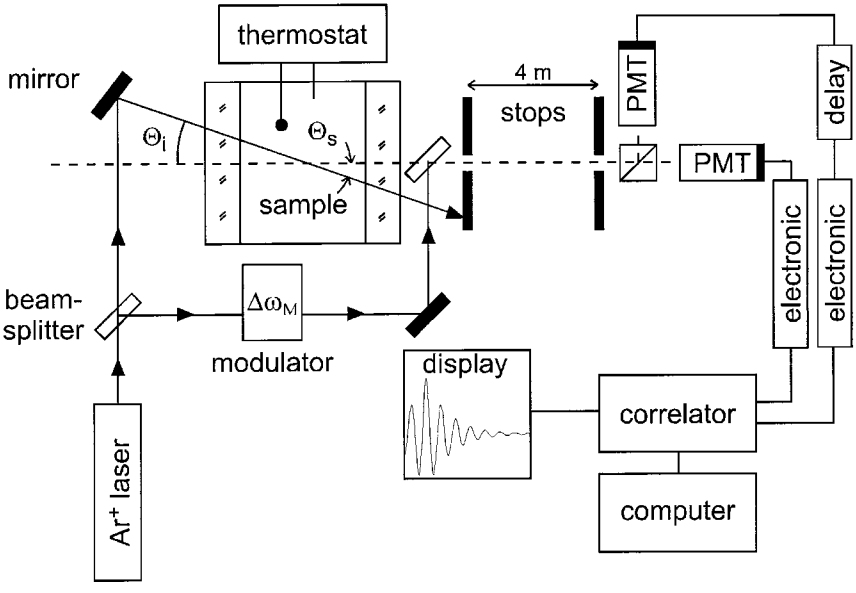

Fig. 2. Experimental setup.

light behind the sample cell. Additionally, for the determination of sound velocity, the reference beam can be shifted in frequency by a single opto-acoustic modulator or by a combination of modulators to reach the desired frequency shift $\Delta\omega_M$. The scattered light intensities are detected by two photomultiplier tubes (PMT's), and the cross-correlation function employed in order to suppress after-pulsing effects, is calculated by a digital correlator. A stand-alone correlator with 112 linearily spaced channels was used with a sample time of 100 ns for the determination of sound speed. For the measurement of thermal diffusivity, the sample time was chosen in a way that the correlation function covers about six times the exponential decay constant.

With the help of Snell's refraction law and simple trigonometric identities, it can be shown that from the angle of incidence Θ_i, which is defined as the angle between the optical axes of incidence laser beam and detection direction (see Fig. 2), the scattering vector q can be deduced to be

$$q \cong \frac{2\pi}{\lambda_0} \sin \Theta_i \tag{7}$$

and can thus be calculated without knowledge of the refractive index n of the sample. The error in the desired quantities resulting from the approximation of Eq. (7) is below 0.1% for angles of incidence up to 5 degrees. In the present experiments the angle of incidence has been measured with an uncertainty of approximately ± 0.014 degree by back-reflection from a mirror, mounted on a precision rotary table.

According to the analysis of the manufacturer (Solvay Fluor und Derivate GmbH, Hannover), the refrigerant sample had a purity of 99.99% and was used without further purification. The sample was filled from the vapor phase into an evacuated cylindrical pressure vessel (volume, $\approx 10\ cm^3$) equipped with two quartz windows (Herasil I; diameter, 30×30 mm). The actual temperature in the sample cell, which was placed in a multi-stage thermostat surrounded by an insulating housing, was regulated through resistance heating and showed a long-term stability of better than ± 0.002 K. The temperature of the sample was measured to within an uncertainty of ± 0.015 K with three calibrated 25-Ω platinum resistance probes, integrated in the main body of the measuring cell. For temperatures below room temperature, the insulating housing was cooled about 10 K below the desired temperature in the sample cell. For each temperature point, typically six measurements at different angles of incidence were performed, where the laser was irradiated from either side with respect to the axis of observation in order to check for a possible misalignment.

4. RESULTS AND DISCUSSION

4.1. Thermal Diffusivity

The results of the measurements of the thermal diffusivity for the saturated liquid and vapor phases are summarized in Table I and Fig. 3. Each temperature point comprises six single measurements, the mean value of which is displayed. The continuous lines are empirical correlations of the experimental data. Either data set can—within experimental uncertainty—be represented by the sum of a polynomial and an additional term that explicitly accounts for the critical behavior,

$$a = \sum_{i=0}^{3} a_i \left(\frac{T}{\mathrm{K}}\right)^i + a_4 \left(\frac{T_c - T}{T_c}\right)^{0.67} \tag{8}$$

where the critical temperature of $T_c = 346.25$ K was taken from Ref. 9. This value is in agreement with the observed maximum opalescence of the sample

Table I. Experimental Values of the Thermal Diffusivity a of R143a (1,1,1-Trifluoroethane) Under Saturation Conditions

Liquid phase		Vapor phase	
T (K)	a (10^{-8} m$^2 \cdot$ s^{-1})	T (K)	a (10^{-8} m$^2 \cdot$ s^{-1})
273.05	5.25	318.12	10.32
283.30	4.79	320.57	9.38
293.03	4.52	323.10	8.60
298.10	4.32	325.60	7.70
303.15	4.19	328.10	6.83
308.13	4.00	330.59	5.87
313.10	3.86	333.10	5.00
318.07	3.65	335.59	4.13
323.03	3.43	338.09	3.24
328.01	3.15	341.09	2.16
330.09	2.96	343.08	1.33
333.09	2.71	344.08	0.941
336.09	2.39	345.08	0.527
338.09	2.15		
340.08	1.83		
341.08	1.64		
342.08	1.42		
343.08	1.16		
344.08	0.846		
345.08	0.462		

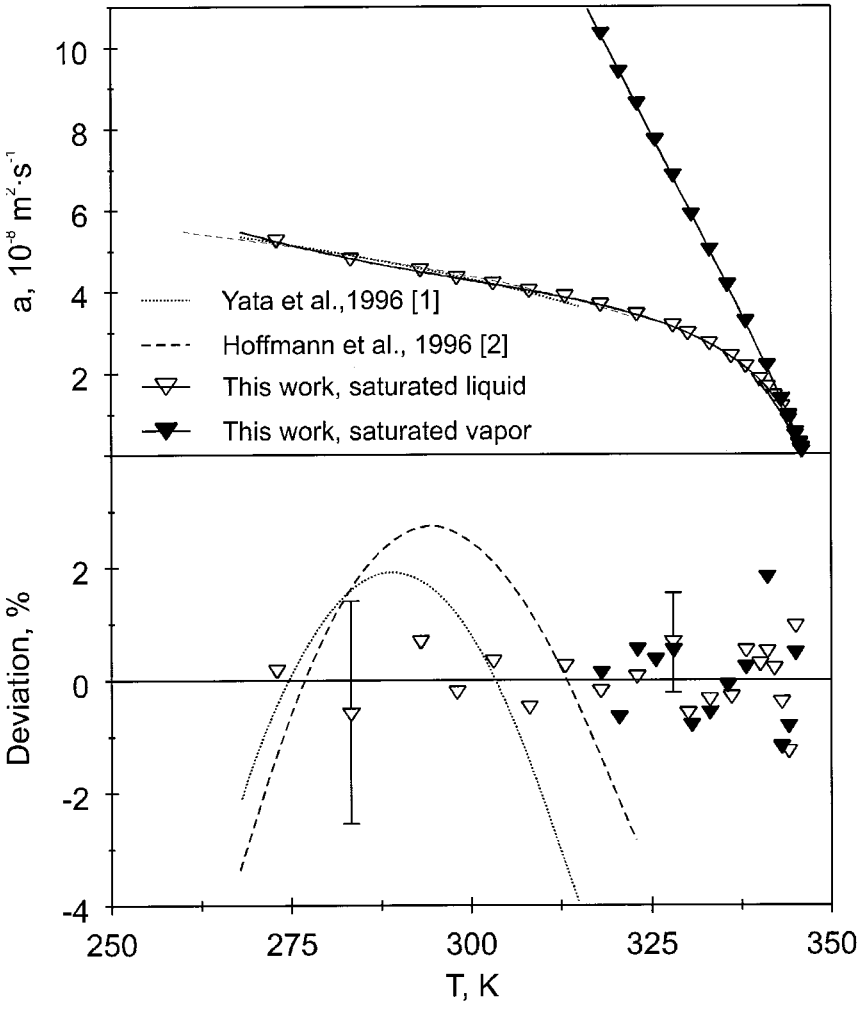

Fig. 3. Thermal diffusivity of saturated R143a.

at a temperature of 346.22 ± 0.03 K. Table II summarizes the coefficients of Eq. (8) for either phase under saturation conditions. Here, also the root-mean square deviations of our values from Eq. (8) and the ranges of validity of the correlations are stated.

In the residual plot of Fig. 3 for the liquid phase, two typical error bars are depicted, which represent the standard deviation of the single measurements and which may be regarded as a measure for the uncertainty of DLS data [10]. For the saturated liquid, a standard deviation of about

Table II. Coefficients of Eq. (8)

a_i ($10^{-8}\,m^2 \cdot s^{-1}$)	Liquid phase	Vapor phase
a_0	49.5183	142.7971
a_1	−0.733715	−0.558964
a_2	2.288873×10^{-3}	0.422476×10^{-3}
a_3	-1.695681×10^{-6}	—
a_4	56.455	13.812
rms (%)	0.53	0.77
T-range (K)	273–345	318–345

2% was obtained for temperatures below 300 K and typically less than 1% for temperatures above 300 K. The observed behavior can be explained because of the increasing signal amplitude for higher temperatures. A corresponding observation regarding the standard deviation holds for the saturated vapor phase. In approaching the critical point, the standard deviation increases again to a value of about 2%, which is due to increasing experimental complexities in the critical region. Thus, investigations in the close vicinity of the gas-liquid critical point require additional effort, which was not done here. Furthermore, due to long measurement times at lower temperatures, the data for the thermal diffusivity in the vapor phase had to be restricted to temperatures above 318 K.

In Fig. 3, for the saturated liquid, reference data from thermal conductivity measurements have been included, which have been converted to thermal diffusity according to

$$a = \frac{\lambda}{\rho c_{\mathbf{P}}} \tag{9}$$

using values for the isobaric heat capacity $c_{\mathbf{P}}$ of Günther and Steimle [11] and for the density ρ of Widiatmo et al. [12]. A direct comparison is not possible for either phase due to a lack of corresponding reference data for the thermal diffusivity. For the boiling liquid, the thermal conductivity data of Yata et al. [1] and Hoffmann et al. [2], both of them obtained by the transient hot-wire method, deviate from our correlation in a range of about −4% to +3%. These differences are within the combined uncertainties of the methods, if one takes into account the uncertainty of the heat capacity data of less than 1% for temperatures up to 313 K and less than 2% for the temperature range between 313 to 323 K, according to Ref. 11. The basically similar course of the deviations for either data set is observed in the correlation of the thermal conductivity data through a linear regression in temperature by the respective authors.

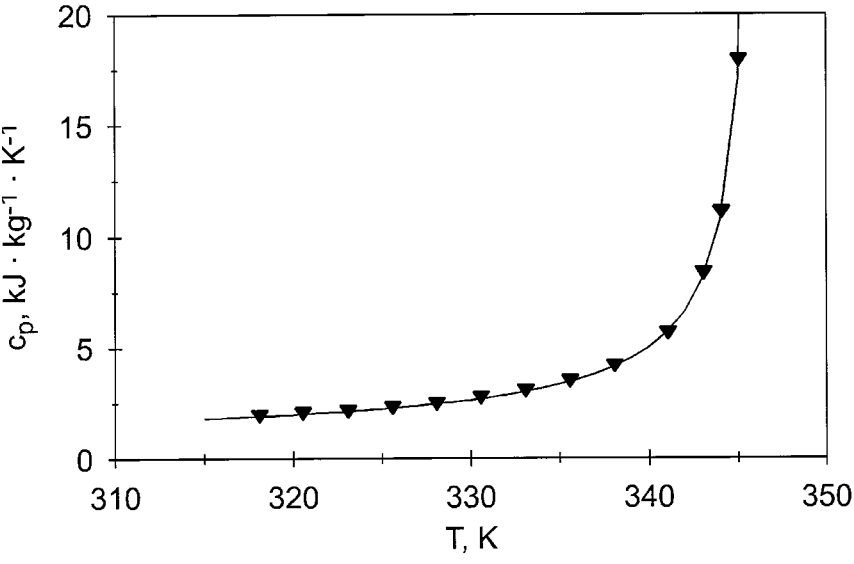

Fig. 4. Specific heat capacity at constant pressure of saturated vapor R143a derived from the experimental values of the thermal diffusivity and with reference data for the thermal conductivity [3] and density [13].

For the thermal diffusivity of the vapor phase at saturation, a data comparison has not been possible due to a lack of values for the isobaric heat capacity. On the other hand a derivation of this quantity at saturation is possible with the present thermal diffusivity data and with the help of reference data for the thermal conductivity and the density in the vapor phase; see, e.g., Refs. 3 and 13, respectively. The result of this procedure is shown in Fig. 4.

4.2. Sound Speed

Our results from dynamic light scattering for the sound speed of saturated R143a are summarized in Table III and Fig. 5. The sound speed data for both vapor and liquid phases can well be represented by a sum of a linear and an additional term, which takes into account the curvature towards the critical point, resulting in an equation of the form,

$$c_S = c_0 + c_1 \left(\frac{T}{K}\right) + c_2 \left(\frac{T_c - T}{T_c}\right)^{\varphi} \tag{10}$$

where the coefficients c_i and the additional fit parameter φ are given in Table IV. The critical temperature again was adopted from Ref. 9. For both

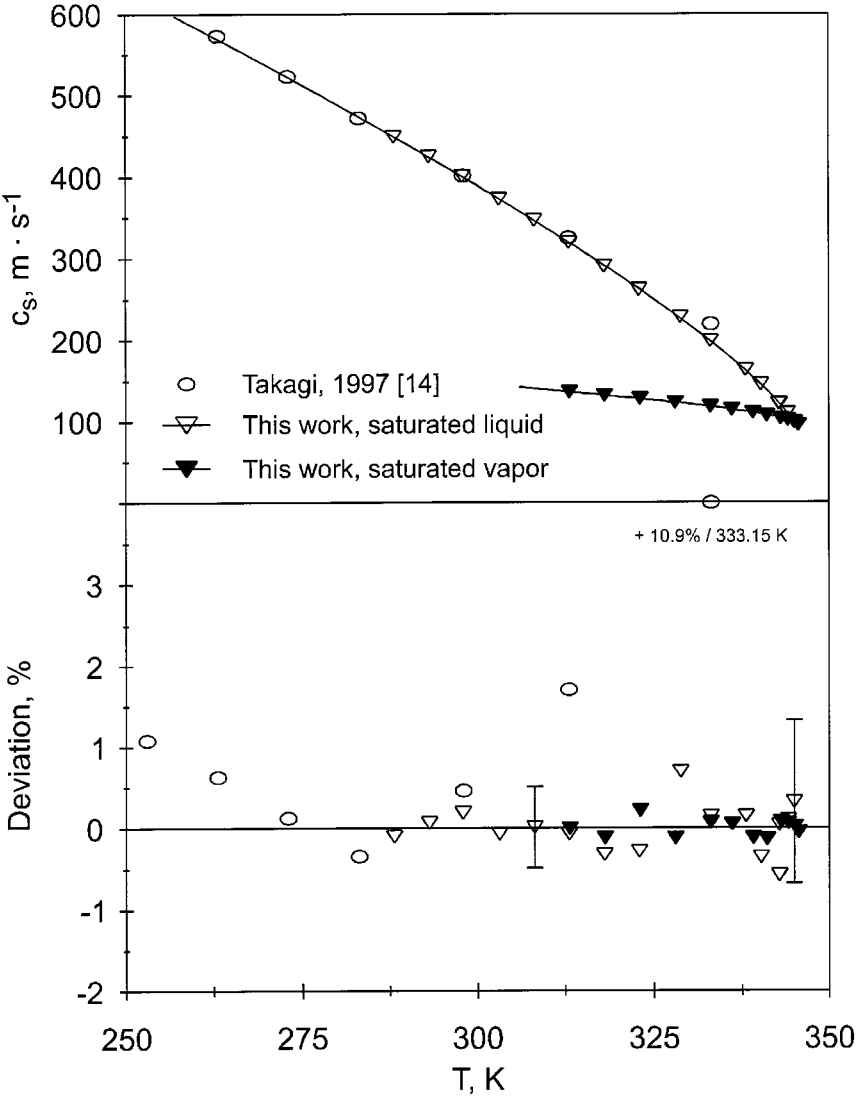

Fig. 5. Sound speed of saturated R143a.

phases the root-mean-square deviation of our data from the fit according to Eq. (10) is clearly less than 0.5% over the whole temperature range.

Taking into account the major error sources, the uncertainty of the sound speed data for temperatures not too close to the critical point ($T/T_c < 0.99$) can be estimated to be less than $\pm 0.5\%$. For the highest

Table III. Experimental Values of the Sound Speed c_S of R143a (1,1,1-Trifluoroethane) Under Saturation Conditions

Liquid phase		Vapor phase	
T (K)	c_S ($m \cdot s^{-1}$)	T (K)	c_S ($m \cdot s^{-1}$)
288.11	449.5	313.13	136.8
293.11	425.2	318.12	132.4
297.95	401.0	323.11	128.5
303.14	373.0	328.10	123.4
308.10	347.0	333.10	118.5
313.06	319.7	336.10	115.0
318.03	291.0	339.10	111.0
322.98	262.3	341.10	107.9
328.80	228.8	343.10	104.4
333.09	199.4	344.10	101.9
338.09	163.5	345.10	98.45
340.23	145.7	345.60	95.79
342.84	123.1		
342.90	121.7		
344.04	110.8		
344.99	99.77		

temperatures studied in this work, the overall uncertainty for the sound speed increases to about 1% as represented by the error bars in Fig. 5. The reason for this behavior can again be found by an increasing experimental complexity in the critical region. It should also be noted that the measured sound speeds are naturally not in the thermodynamic $\omega_S = 0$ limit, and thus, dispersion might affect both the average values and the standard deviation.

For comparison of the sound speed of the liquid phase under saturation conditions, only one data set is available in the literature. These are

Table IV. Coefficients of Eq. (10)

c_i ($m \cdot s^{-1}$)	Liquid phase	Vapor phase
c_0	978.29	281.696
c_1	−2.6095	−0.60365
c_2	665.96	65.547
φ	0.612	0.1685
rms (%)	0.29	0.10
T-range (K)	288–345	313–345

estimated values by Takagi [14], where the sound velocity on the saturation line is obtained by extrapolating experimental data for the compressed liquid phase measured with an ultrasonic acoustic interferometer. In Ref. 14 an estimated uncertainty of $\pm 0.2\%$ for the experimental values in the high density region is stated, yet due to absorption effects at higher temperatures near the saturation region a larger error, especially for the sound speed below $400\ \mathrm{m \cdot s^{-1}}$, is noted. These facts may explain that at a temperature of about 300 K, where the sound speed is $400\ \mathrm{m \cdot s^{-1}}$, an increasing difference between our data and the estimation given by Takagi can be observed with increasing temperature, see Fig. 5. Since far away from the critical point, Eq. (10) well represents the quasi-linear temperature dependence of the saturated liquid sound speed, we have extrapolated our correlation for temperatures down to 250 K. Here, better agreement can be found between the extrapolated data and those of Takagi [14].

Although experimental data exist in the literature for gas-phase sound speeds of R143a, see, e.g., Ref. 15, no data are available for the saturation line. Thus, no data comparisons were performed here.

5. CONCLUSIONS

For the refrigerant R143a, which serves as a principal component in the refrigerant blends R507 and R404A, the thermal diffusivity and sound speed have been measured using dynamic light scattering. Values have been determined for both the liquid and vapor phases under saturation conditions over a wide temperature range up to the critical point. For a limited range at moderate temperatures, where reference data in the liquid phase are available for density, thermal conductivity, and the specific heat, comparisons with our thermal diffusivity data show agreement within the cumulative uncertainties of the single properties used for data conversion. In the high temperature range, a comparison of our results obtained for the thermal diffusivity and sound velocity was not possible because of the lack of other data sets in this region. Here, experiments by other techniques would be most helpful. For the thermal diffusivity and sound speed of R143a, to the best of our knowledge, the present results from dynamic light scattering are the first experimental values under saturation conditions.

ACKNOWLEDGMENTS

Part of the work was financially supported by the Deutsche Forschungsgemeinschaft (DFG). The authors gratefully acknowledge the help of Solvay Fluor und Derivate GmbH, Hannover by providing the refrigerant sample and analyzing its purity.

REFERENCES

1. J. Yata, M. Hori, K. Kobayashi, and T. Minamiyama, *Int. J. Thermophys.* **17**:561 (1996).
2. N. Hoffmann, K. Spindler, and E. Hahne, *Bestimmung der Transportgrven von HFKW*, Bericht zum AiF-Forschungsvorhaben Nr. 10044B, Forschungsrat Kältetechnik e.V. (Frankfurt, 1996), pp. 23–24.
3. Y. Tanaka, M. Nakata, and T. Makita, *Int. J. Thermophys.* **12**:949 (1991).
4. A. Leipertz, *Fluid Phase Equil.* **125**:219 (1996).
5. S. Will and A. Leipertz, in *Diffusion in Condensed Matter*, J. Kärger, P. Heitjans, and R. Haberlandt, eds. (Vieweg, Wiesbaden, Germany, 1999), pp. 219–244.
6. B. J. Berne and R. Pecora, *Dynamic Light Scattering* (John Wiley, New York, 1976).
7. B. Chu, *Laser Light Scattering* (Academic Press, New York, 1991).
8. K. Kraft and A. Leipertz, *Int. J. Thermophys.* **16**:445 (1995).
9. M. O. McLinden, *Int. J. Refrig.* **13**:149 (1990).
10. K. Kraft, M. Matos Lopes, and A. Leipertz, *Int. J. Thermophys.* **16**:423 (1995).
11. D. Günther and D. Steimle, *DKV-Tagungsbericht* 23 (Leipzig, 1996), Vol. II.1, pp. 261–272.
12. J. V. Widiatmo, H. Sato, and K. Watanabe, *J. Chem. Eng. Data* **39**:304 (1994).
13. K. Srinivasan and L. R. Oellrich, *Int. J. Refrig.* **20**:332 (1997).
14. T. Takagi, *J. Chem. Eng. Data* **42**:1129 (1997).
15. K. A. Gillis, *Int. J. Thermophys.* **18**:73 (1997).